Role of the triangle singularity in $\Lambda(1405)$ production in the $\pi^- p \to K^0 \pi \Sigma$ and $pp \to p K^+ \pi \Sigma$ processes

M. Bayar,[1,2,*] R. Pavao,[2] S. Sakai,[2] and E. Oset[2]

[1]*Department of Physics, Kocaeli University, 41380 Izmit, Turkey*

[2]*Departamento de Física Teórica and IFIC, Centro Mixto Universidad de Valencia-CSIC Institutos de Investigación de Paterna, Aptdo.22085, 46071 Valencia, Spain*

(Received 24 October 2017; revised manuscript received 8 January 2018; published 7 March 2018)

We have investigated the cross section for the $\pi^- p \to K^0 \pi \Sigma$ and $pp \to p K^+ \pi \Sigma$ reactions, paying attention to a mechanism that develops a triangle singularity. The triangle diagram is realized by the decay of a N^* to $K^* \Sigma$ and the K^* decay into πK, and the $\pi \Sigma$ finally merges into $\Lambda(1405)$. The mechanism is expected to produce a peak around 2140 MeV in the $K \Lambda(1405)$ invariant mass. We found that a clear peak appears around 2100 MeV in the $K \Lambda(1405)$ invariant mass, which is about 40 MeV lower than the expectation, and that is due to the resonance peak of a N^* resonance which plays a crucial role in the $K^* \Sigma$ production. The mechanism studied produces the peak of the $\Lambda(1405)$ around or below 1400 MeV, as is seen in the $pp \to p K^+ \pi \Sigma$ HADES experiment.

DOI: 10.1103/PhysRevC.97.035203

I. INTRODUCTION

The nature of $\Lambda(1405)$, the lowest excitation of Λ with $J^P = 1/2^-$, has been given much attention for a long time. The quark model predicts the mass at higher energy than the observed peak [1], and a description of $\Lambda(1405)$ as a $\bar{K} N$ molecular state shows a good agreement with the experimental result, as originally pointed out in Refs. [2–4]. The studies of the $\bar{K} N$ system based on SU(3) chiral symmetry with the implementation of unitarity and coupled channels suggest that $\Lambda(1405)$ is generated as a $\bar{K} N$ quasibound state [5–16]. The recent analysis of the lattice QCD simulation supports the molecular picture of $\Lambda(1405)$ [17,18]. Furthermore, the analysis of the compositeness [19–21], which is a measure of the hadronic molecular component, the charge radius [22], and the root mean square radius [23], also supports the picture of $\Lambda(1405)$ as a $\bar{K} N$ molecule. Other than these works, many studies of $\Lambda(1405)$ production from photon-induced reactions [24–29], pion-induced reactions [30,31], kaon-induced reactions [32–35], proton-proton collisions [36,37], and heavy meson decay [38] were carried out to clarify the nature of the $\Lambda(1405)$ resonance. The studies related to the $\bar{K} N$ system are summarized in Refs. [39,40] (see also the note "Pole Structure of the $\Lambda(1405)$ Region" by U.-G. Meissner and T. Hyodo in PDG [41]).

In Ref. [29], the role of the triangle singularity (TS) on the angle and the energy dependence of $\Lambda(1405)$ photoproduction was studied. The triangle singularity was first pointed out in Ref. [42]. The corresponding Feynman diagram is formed by a sequential decay of a hadron and a fusion of two of them, and the amplitude associated with the diagram has a singularity if the process has a classical counterpart, which is known as the Coleman–Norton theorem [43]. The studies of many processes including the triangle singularity elucidate the possible effect of the triangle singularity on the hadron properties, *e.g.*, the $\eta(1405)$ decay into $\pi^0 a_0$ or $\pi^0 f_0$ [44–46], the possible origin of $Z_c(3900)$ [47–49], the speculation on the pentaquark candidate P_c [50–52] (see Ref. [53] for a critical discussion to the light of the preferred experimental quantum numbers [54]), the B_s decay into $B \pi \pi$ [55] and B^- decays [56,57]. Here, we note that the strength of the triangle peak is tightly connected with the coupling strength of the two hadrons merging into a third one. For example, in the study of the B^- decay into $K^- \pi^- D_{s0}^+ (D_{s1}^+)$ [56], the DK $(D^* K)$ in the triangle loop goes into D_{s0} (D_{s1}), which is dynamically generated from the DK $(D^* K)$ and has a large coupling to this channel [58,59]. Then, the observation of the peak from the triangle mechanism would give additional support to the hadronic molecular picture of these states.

For further understanding of the nature of $\Lambda(1405)$ and triangle mechanisms, in this paper we investigate the $\pi^- p \to K^0 \pi \Sigma$ and $pp \to p K^+ \pi \Sigma$ processes including a triangle diagram. In both processes, the triangle diagram is formed by a N^* decay into $K^* \Sigma$ followed by the decay of K^* into πK and the fusion of $\pi \Sigma$ to form $\Lambda(1405)$, which finally decays into $\pi \Sigma$. In this process, the $K^* \pi \Sigma$ loop generates a triangle singularity around 2140 MeV in the invariant mass of $K \Lambda(1405)$ from the formula given by Eq. (18) of Ref. [53]. The corresponding diagram is shown in Fig. 1. The N^* resonance, which strongly couples to $K^* \Sigma$, is obtained in Ref. [60] based on the hidden local symmetry and the chiral unitary approach, and the analysis of the $K \Sigma$ photoproduction off nucleon around the $K^* \Lambda$ threshold energy suggests that the resonance is responsible for the observed cross section [61].

*melahat.bayar@kocaeli.edu.tr

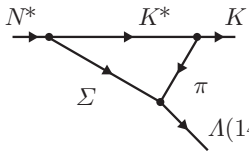

FIG. 1. Triangle diagram for $\Lambda(1405)$ production from a N^* resonance.

As the result of our calculation, we find a peak in the $K\Lambda(1405)$ mass distribution around 2100 MeV in both reactions, which is lowered with respect to the 2140 MeV given by the TS master formula [53] by the initial N^* resonance which peaks around 2030 MeV. The experimental study on $\Lambda(1405)$ production from $\pi^- p$ is reported in Refs. [62,63], but the energy is too small for the triangle singularity from the $K^*\pi\Sigma$ loop to be observed. The production of $\Lambda(1405)$ from the proton-proton collision is studied in Refs. [64–66]. The future observation of the inevitable peak from the triangle mechanism induced by $\Lambda(1405)$ would give further support for the molecular nature of $\Lambda(1405)$.

II. FORMALISM

A. $\pi^- p \to K^0 \pi \Sigma$

In this section we study the effects of the triangle loop in the following decays: $\pi^- p \to K^0\pi^+\Sigma^-$, $\pi^- p \to K^0\pi^0\Sigma^0$, and $\pi^- p \to K^0\pi^-\Sigma^+$. The diagrams where the triangle singularity can appear for those reactions are shown in Fig. 2. To evaluate the differential cross section associated with this diagram, we use

$$\frac{d\sigma_{K^0\pi\Sigma}}{dm_{\rm inv}} = \frac{M_p M_\Sigma |\vec{k}||\vec{p}_\pi|}{2(2\pi)^3 s|\vec{p}_\pi|}\overline{\sum}\sum |t_{\pi^- p\to K^0\pi\Sigma}|^2, \quad (1)$$

with $m_{\rm inv}$ being the invariant mass of the final $\pi\Sigma$,

$$|\vec{p}_\pi| = \frac{\lambda^{\frac{1}{2}}\left(s, m_\pi^2, M_N^2\right)}{2\sqrt{s}}, \quad (2)$$

the momentum of the initial π^- in the $\pi^- p$ center-of-mass (c.m.) frame,

$$|\vec{k}| = \frac{\lambda^{\frac{1}{2}}\left(s, m_K^2, m_{\rm inv}^2\right)}{2\sqrt{s}}, \quad (3)$$

the momentum of the final K^0 in the $\pi^- p$ c.m., and

$$|\vec{\tilde{p}}_\pi| = \frac{\lambda^{\frac{1}{2}}\left(m_{\rm inv}^2, m_\pi^2, M_\Sigma^2\right)}{2m_{\rm inv}}, \quad (4)$$

the momentum of the final π in the $\pi\Sigma$ c.m.

The resonance $N^*(2030)$ studied in Ref. [60] from the vector-baryon interaction, mediated by the exchange of vector mesons, appears there as spin degenerate in $J^P = 1/2^-$ and $3/2^-$. The degeneracy can be broken by mixing with states of pseudoscalar-baryon and connecting these by pion exchange, as done in Ref. [67]. There should be then two states near degenerate at the end. We conduct our study with the $J^P = 1/2^-$ state. The case of spin $3/2^-$ is discussed at the end of this section. For the moment it is sufficient to mention that the structure and conclusions for that term are the same as for the $1/2^-$ state.

In the isospin basis, the $\pi^- p \to N^*$ vertex has the form

$$-it_{\pi N,N^*} = -ig^{I=\frac{1}{2}}_{\pi N,N^*}. \quad (5)$$

To estimate the $g^{I=\frac{1}{2}}_{\pi N,N^*}$ we assume that $\Gamma_{N^*,\pi N}$ is of the order of 70 MeV and then use the formula

$$\Gamma_{N^*,\pi N} = \frac{1}{2\pi}\frac{M_\Sigma}{M_{N^*}}\left(g^{I=\frac{1}{2}}_{\pi N,N^*}\right)^2 |\vec{p}_\pi|, \quad (6)$$

with M_{N^*} being the mass of $N^*(2030)$. Here, $|\vec{p}_\pi|$ is the momentum of π that results from the decay of N^* and is evaluated by using Eq. (2), $s = M_{N^*}^2$. Finally, we obtain $g^{I=\frac{1}{2}}_{\pi N,N^*} \simeq 1.1$.

The value of $\Gamma_{N^*,\pi N} = 70$ MeV is just an estimate. We should warn here that we are not so much interested in the strength of the cross section, which we cannot evaluate accurately in this formalism. One reason is precisely that $\Gamma_{N^*,\pi N}$ is not known. Yet, the important thing is the shape of the invariant-mass distribution and, as we shall see later on, we also prove that the triangle mechanism is more important than tree-level mechanisms. The estimate of 70 MeV is based on values that we get from the old version of the PDG [68], for two states $N^*(2080)(3/2^-)$ and $N^*(2090)(1/2^-)$ and the original papers of Refs. [69,70] and Ref. [71], playing with very large errors in both experiments.

Since we will have different amplitudes if we change the charge of the intermediate $\pi\Sigma$ particles, it is convenient to go from the isospin basis ($|I, I_3\rangle$) to the charge basis. Although a formalism using the different $\pi\Sigma$ isospin channels is possible, we find it convenient to work in the charge basis. Using the

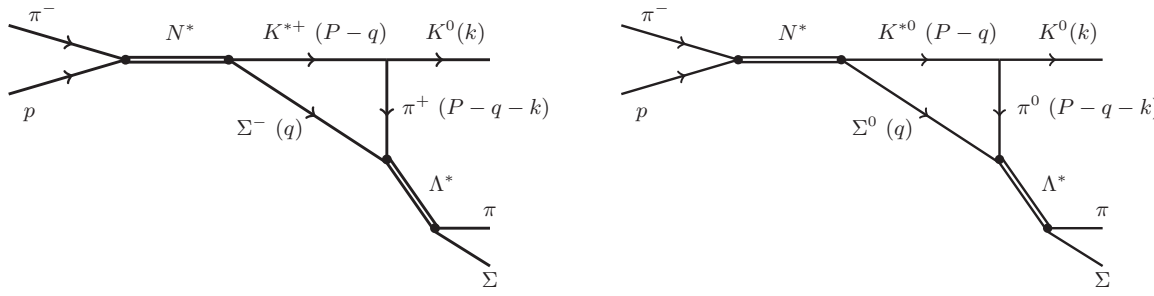

FIG. 2. Diagrams for the reaction $\pi^- p \to K^0\pi\Sigma$ that contains the triangle mechanism, where $\pi\Sigma$ can be $\pi^-\Sigma^+$, $\pi^0\Sigma^0$, or $\pi^+\Sigma^-$.

Clebsch–Gordan coefficients, we have

$$|\pi^- p\rangle = \sqrt{\frac{1}{3}}\left|\frac{3}{2},-\frac{1}{2}\right\rangle - \sqrt{\frac{2}{3}}\left|\frac{1}{2},-\frac{1}{2}\right\rangle. \tag{7}$$

This means that the coupling of $\pi^- p$ to N^* will be

$$g_{\pi^- p,N^*} = -\sqrt{\frac{2}{3}} g^{I=\frac{1}{2}}_{\pi N,N^*}. \tag{8}$$

For the $N^*(2030) \to K^*\Sigma$ process in s wave, as shown in the appendix for spin $J = 1/2$, we have

$$-it_{N^*,K^*\Sigma} = -i\frac{1}{\sqrt{3}} g_{N^*,\Sigma K^*}\vec{\sigma}\cdot\vec{\epsilon}_{K^*}. \tag{9}$$

From Ref. [60], we get $g^{I=\frac{1}{2}}_{N^*,K^*\Sigma} = 3.9 + i0.2$, and since we have both $\Sigma^- K^{*+}$ and $\Sigma^0 K^{*0}$ [Figs. 2(a) and 2(b), respectively], then, using

$$|\Sigma^0 K^{*0}\rangle = \sqrt{\frac{2}{3}}\left|\frac{3}{2},-\frac{1}{2}\right\rangle + \sqrt{\frac{1}{3}}\left|\frac{1}{2},-\frac{1}{2}\right\rangle, \tag{10a}$$

$$|\Sigma^- K^{*+}\rangle = \sqrt{\frac{1}{3}}\left|\frac{3}{2},-\frac{1}{2}\right\rangle - \sqrt{\frac{2}{3}}\left|\frac{1}{2},-\frac{1}{2}\right\rangle, \tag{10b}$$

we get

$$g_{N^*,\Sigma^0 K^{*0}} = \sqrt{\frac{1}{3}} g^{I=\frac{1}{2}}_{N^*,\Sigma K^*}, \tag{11a}$$

$$g_{N^*,\Sigma^- K^{*+}} = -\sqrt{\frac{2}{3}} g^{I=\frac{1}{2}}_{N^*,\Sigma K^*}. \tag{11b}$$

Then, for the amplitude of the $\pi^- p \to \Sigma K^*$ reaction through $N^*(2030)$, we have

$$t_{\pi^- p,\Sigma^0 K^{*0}} = \frac{1}{\sqrt{3}} \frac{g_{\pi^- p,N^*} g_{N^*,\Sigma^0 K^{*0}}}{\sqrt{s} - M_{N^*} + i\frac{\Gamma_{N^*}}{2}} \vec{\sigma}\cdot\vec{\epsilon}_{K^*}, \tag{12a}$$

$$t_{\pi^- p,\Sigma^- K^{*+}} = \frac{1}{\sqrt{3}} \frac{g_{\pi^- p,N^*} g_{N^*,\Sigma^- K^{*+}}}{\sqrt{s} - M_{N^*} + i\frac{\Gamma_{N^*}}{2}} \vec{\sigma}\cdot\vec{\epsilon}_{K^*}. \tag{12b}$$

Now, the $K^{*+} \to K^0\pi^+$ vertex can be calculated by using the chiral invariant Lagrangian with the local hidden symmetry given in Refs. [72–75],

$$\mathcal{L}_{VPP} = -ig\langle[\Phi,\partial_\mu\Phi]V^\mu\rangle. \tag{13}$$

The symbol $\langle\ldots\rangle$ here represents the trace over the SU(3) flavor matrices, and the coupling is $g = m_V/2f_\pi$, with $m_V = 800$ MeV and $f_\pi = 93$ MeV. The SU(3) matrices for the pseudoscalar and vector octet mesons Φ and V^μ are given by

$$\Phi = \begin{pmatrix} \frac{1}{\sqrt{2}}\pi^0 + \frac{1}{\sqrt{6}}\eta & \pi^+ & K^+ \\ \pi^- & -\frac{1}{\sqrt{2}}\pi^0 + \frac{1}{\sqrt{6}}\eta & K^0 \\ K^- & \bar{K}^0 & -\sqrt{\frac{2}{3}}\eta \end{pmatrix}, \tag{14}$$

$$V_\mu = \begin{pmatrix} \frac{1}{\sqrt{2}}\rho^0_\mu + \frac{1}{\sqrt{2}}\omega_\mu & \rho^+_\mu & K^{*+}_\mu \\ \rho^-_\mu & -\frac{1}{\sqrt{2}}\rho^0_\mu + \frac{1}{\sqrt{2}}\omega_\mu & K^{*0}_\mu \\ K^{*-}_\mu & \bar{K}^{*0}_\mu & \phi_\mu \end{pmatrix}. \tag{15}$$

From Eq. (13) we get

$$-it_{K^{*+},K^0\pi^+} = -ig\epsilon^\mu_{K^*}(p_{K^0} - p_{\pi^+})_\mu \tag{16}$$

$$= ig\epsilon^\mu_{K^*}(P - q - 2k)_\mu \tag{17}$$

$$\simeq ig\vec{\epsilon}_{K^*}\cdot(\vec{q} + 2\vec{k}), \tag{18}$$

where in the last step we made a nonrelativistic approximation by neglecting the $\epsilon^0_{K^*}$ component. This is very accurate when the momentum of the K^* is small compared with its mass. We shall evaluate the triangle diagram in the ΣK^* c.m., where the on-shell momentum of the K^* is about 250 MeV/c at $M_{\rm inv}(\Sigma K^*) \simeq 2140$ MeV where the triangle singularity appears. In Ref. [56] it is shown that the effect of neglecting the ϵ^0 component goes as $(p_{K^*}/m_{K^*})^2$, with a coefficient in front that renders this correction negligible.

Similarly, for $K^{*0} \to K^0\pi^0$ we get

$$-it_{K^{*0},K^0\pi^0} = -i\frac{1}{\sqrt{2}} g\vec{\epsilon}_{K^*}\cdot(\vec{q} + 2\vec{k}). \tag{19}$$

The final vertex that we need to calculate in the diagrams of Fig. 1 is $t_{\Sigma\pi,\Sigma\pi}$ which is given by the $\Sigma\pi \to \Lambda(1405) \to \Sigma\pi$ amplitude studied in Ref. [6] based on the chiral unitary approach. There, the authors use the lowest-order meson-baryon chiral Lagrangian

$$\mathcal{L}^{(B)}_1 = \left\langle \bar{B} i\gamma^\mu \frac{1}{4f^2}[(\Phi\partial_\mu\Phi - \partial_\mu\Phi\Phi)B - B(\Phi\partial_\mu\Phi - \partial_\mu\Phi\Phi)]\right\rangle, \tag{20}$$

with

$$B = \begin{pmatrix} \frac{1}{\sqrt{2}}\Sigma^0 + \frac{1}{\sqrt{6}}\Lambda & \Sigma^+ & p \\ \Sigma^- & -\frac{1}{\sqrt{2}}\Sigma^0 + \frac{1}{\sqrt{6}}\Lambda & n \\ \Xi^- & \Xi^0 & -\sqrt{\frac{2}{3}}\Lambda \end{pmatrix}. \tag{21}$$

The Bethe–Salpeter equation is then used to calculate the meson-baryon amplitude,

$$t = [1 - VG]^{-1}V, \tag{22}$$

where t, V, and G are the meson-baryon amplitude, interaction kernel, and meson-baryon loop function, respectively. For the evaluation of t, we use the momentum cutoff $q_{\rm max} = 630$ MeV for the loop function G, and $f = 1.15 f_\pi$ with the pion-decay constant $f_\pi = 93$ MeV as done in Ref. [6].

Thus, the amplitude associated with the diagram in Fig. 2(a), which we call t_1, is given by

$$t_1 = -i\frac{2}{3\sqrt{3}} \frac{g^{I=\frac{1}{2}}_{\pi N,N^*} g^{I=\frac{1}{2}}_{N^*,\Sigma K^*}}{\sqrt{s} - M_{N^*} + i\frac{\Gamma_{N^*}}{2}} g \sum_{\text{pol. of } K^*} \int \frac{d^4q}{(2\pi)^4} \frac{2M_\Sigma \vec{\sigma}\cdot\vec{\epsilon}_{K^*}}{q^2 - M^2_\Sigma + i\epsilon} \frac{(2\vec{k} + \vec{q})\cdot\vec{\epsilon}_{K^*}}{(P - q)^2 - m^2_{K^*} + i\epsilon} \frac{t_{\Sigma^-\pi^+,\Sigma\pi}}{(P - q - k)^2 - m^2_\pi + i\epsilon}. \tag{23}$$

Using the property

$$\int d^3q q_i f(\vec{q},\vec{k}) = k_i \int d^3q \frac{\vec{q}\cdot\vec{k}}{|\vec{k}|^2} f(\vec{q},\vec{k}),$$

with $f(\vec{q},\vec{k})$ being the three propagators in the integrand of Eq. (23), and the formula in the nonrelativistic approximation,

$$\sum_{\text{pol.}} \epsilon_{K^* i}\epsilon_{K^* j} = \delta_{ij},$$

Eq. (23) becomes

$$t_1 = -\frac{4M_\Sigma}{3\sqrt{3}} \frac{g^{I=\frac{1}{2}}_{\pi N,N^*} g^{I=\frac{1}{2}}_{N^*,\Sigma K^*}}{\sqrt{s}-M_{N^*}+i\frac{\Gamma_{N^*}}{2}} g\vec{\sigma}\cdot\vec{k} t_T\, t_{\Sigma^-\pi^+,\Sigma\pi}, \tag{24}$$

with

$$t_T = i\int \frac{d^4q}{(2\pi)^4}\left(2+\frac{\vec{q}\cdot\vec{k}}{|\vec{k}|^2}\right)\frac{1}{q^2-M_\Sigma^2+i\epsilon}\frac{1}{(P-q)^2-m_{K^*}^2+i\epsilon}\frac{1}{(P-q-k)^2-m_\pi^2+i\epsilon}. \tag{25}$$

Integrating t_T over q^0, we get [53,76]

$$t_T = \int \frac{d^3q}{(2\pi)^3}\left(2+\frac{\vec{q}\cdot\vec{k}}{|\vec{k}|^2}\right)\frac{1}{8\omega^*\omega\omega'}\frac{1}{k^0-\omega'-\omega^*}\frac{1}{P^0+\omega+\omega'-k^0}\frac{1}{P^0-\omega-\omega'-k^0+i\epsilon} \times \frac{\{2P^0\omega+2k^0\omega'-2[\omega+\omega'][\omega+\omega'+\omega^*]\}}{P^0-\omega^*-\omega+i\epsilon}, \tag{26}$$

where $P^0=\sqrt{s}$, $\omega^*(\vec{q}\,)=(m_{K^{*0}}^2+|\vec{q}\,|^2)^{1/2}$, $\omega'(\vec{q}\,)=(m_\pi^2+|\vec{q}+\vec{k}|^2)^{1/2}$, and $\omega(\vec{q}\,)=(M_\Sigma^2+|\vec{q}\,|^2)^{1/2}$. We regularize the integral in Eq. (26) by using the same cutoff of the meson loop in Eq. (22), $\theta(q_{\max}-|\vec{q}^{\,*}|)$, where $\vec{q}^{\,*}$ is the Σ momentum in the final $\pi\Sigma$ c.m. [53] and $q_{\max}=630$ MeV. The width of K^* is taken into account by replacing ω^* with $\omega^*-i\frac{\Gamma_{K^*}}{2}$.

For the case when $N^*(2030)\to K^{*+}\Sigma^-$, t_2, we have

$$t_2 = -\frac{2M_\Sigma}{3\sqrt{3}} \frac{g^{I=\frac{1}{2}}_{\pi N,N^*} g^{I=\frac{1}{2}}_{N^*,\Sigma K^*}}{\sqrt{s}-M_{N^*}+i\frac{\Gamma_{N^*}}{2}} g\vec{\sigma}\cdot\vec{k} t_T t_{\Sigma^0\pi^0,\Sigma\pi}. \tag{27}$$

Thus, the total amplitude in Eq. (1) associated with $\pi^- p\to K^0\pi\Sigma$ becomes

$$t_{\pi^- p\to K^0\pi\Sigma} = t_1+t_2 = C\vec{\sigma}\cdot\vec{k} t_T\left(t_{\Sigma^-\pi^+,\Sigma\pi}+\tfrac{1}{2}t_{\Sigma^0\pi^0,\Sigma\pi}\right), \tag{28}$$

with

$$C = -\frac{2}{3\sqrt{3}} g^{I=\frac{1}{2}}_{\pi N,N^*} g^{I=\frac{1}{2}}_{N^*,\Sigma K^*} g \frac{2M_\Sigma}{\sqrt{s}-M_{N^*}+i\frac{\Gamma_{N^*}}{2}}. \tag{29}$$

Here, the t_T associated with the diagrams in Figs. 2(a) and 2(b) are the same because we use the isospin-averaged mass and width of the hadrons in t_T.

Calculating the square of the amplitude and summing and averaging over the spins we get

$$\overline{\sum}\sum |t_{\pi^- p\to K^0\pi\Sigma}|^2 = |C|^2|\vec{k}|^2|t_T|^2\left|t_{\Sigma^-\pi^+,\Sigma\pi}+\frac{1}{2}t_{\Sigma^0\pi^0,\Sigma\pi}\right|^2. \tag{30}$$

Finally, by using Eq. (30) in Eq. (1), we can calculate $d\sigma_{K^0\pi\Sigma}/dm_{\text{inv}}$ associated with the diagrams in Fig. 2.

To incorporate the contribution of spin 3/2, we follow the appendix equations (A11) and (A14) and we see that, instead of

$$\sum_{K^*\text{ pol.}} \frac{1}{3}\vec{\sigma}\cdot\vec{\epsilon}_{K^*}\,\vec{\epsilon}_{K^*}\cdot\vec{k}, \tag{31}$$

we get

$$\sum_{K^*\text{ pol.}} \sigma_3\epsilon_{K^*3}\vec{\epsilon}_{K^*}\cdot\vec{k}. \tag{32}$$

Thus, after summing over the K^* polarizations

$$\tfrac{1}{3}\vec{\sigma}\cdot\vec{k}\to\sigma_3 k_3 \tag{33}$$

and upon squaring it for $|t|^2$ and summing and averaging over the baryon spins, we get

$$\tfrac{1}{9}|\vec{k}|^2\to k_3^2\to\tfrac{1}{3}|\vec{k}|^2, \tag{34}$$

where the last step considers the angular integration over $\vec{k}$ in $d\sigma/dM_{\text{inv}}$.

The conclusion is that the sum of the spin 1/2 and 3/2 is three times bigger than the contribution of $J=1/2$ alone or, equivalently, $J=3/2$ contributes twice the amount of $J=1/2$. This is logical because, in the diagram of Fig. 13, one is summing over two third components of R for $J=1/2$ and over four for $J=3/2$. For practical reasons we can evaluate the whole contribution by using the $J=1/2$ formalism removing the factor $1/\sqrt{3}$ in Eq. (9) and this is what we shall do in what follows.

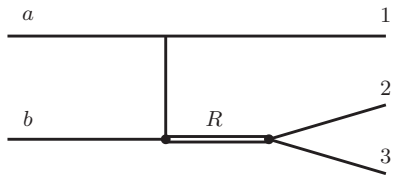

FIG. 3. Diagram of $a\ b \to 1\ R \to 1\ 2\ 3$.

B. $pp \to pK^+\pi\Sigma$

Now we will study the effects of the triangle loop in the following decays: $pp \to pK^+\pi^+\Sigma^-$, $pp \to pK^+\pi^0\Sigma^0$, and $pp \to pK^+\pi^-\Sigma^+$. For this, we first start analyzing the diagram in Fig. 3. For this diagram, the differential cross section is calculated by using the formula in Ref. [77],

$$\frac{d^2\sigma}{dt dM_{\rm inv}} = \frac{\prod_F (2M_F)}{32 p_a^2 s (2\pi)^3} |\vec{\tilde{p}}_2| \overline{\sum} \sum |t_{ab\to 123}|^2, \tag{35}$$

where $t = (p_a - p_1)^2$, $M_{\rm inv}$ is the invariant mass of particles 2 and 3, $\vec{\tilde{p}}_2$ is the momentum of particle 2 in the 23 c.m., such that

$$|\vec{\tilde{p}}_2| = \frac{\lambda^{\frac{1}{2}}\left(M_{\rm inv}^2, m_2^2, m_3^2\right)}{2M_{\rm inv}}, \tag{36}$$

p_a is the momentum of the particle a in the initial state,

$$p_a = \frac{\lambda^{\frac{1}{2}}\left(s, M_a^2, M_b^2\right)}{2\sqrt{s}}, \tag{37}$$

and $\Pi_F(2M_F)$ means that we multiply $2M_F$ for each fermion in Fig. 3, where M_F is the mass of the respective fermion. This factor appears because we use the normalization of Ref. [78].

The complete diagrams for our reaction are shown in Fig. 4. The triangle part of the diagrams is very similar to the last case, except that, because of charge conservation, the particles in the loop will be different. Thus, instead of Eqs. (10a) and (10b), we have

$$|\Sigma^+ K^{*0}\rangle = -\sqrt{\frac{1}{3}}\left|\frac{3}{2},\frac{1}{2}\right\rangle - \sqrt{\frac{2}{3}}\left|\frac{1}{2},\frac{1}{2}\right\rangle, \tag{38a}$$

$$|\Sigma^0 K^{*+}\rangle = \sqrt{\frac{2}{3}}\left|\frac{3}{2},\frac{1}{2}\right\rangle - \sqrt{\frac{1}{3}}\left|\frac{1}{2},\frac{1}{2}\right\rangle, \tag{38b}$$

where, to match the sign convention of the Φ and B matrices, we used $|\Sigma^+\rangle = -|1\ 1\rangle$ (see Ref. [79] for further discussion). Then, we get $g_{N^*,\Sigma^+K^{*0}} = -\sqrt{2/3}\, g^{I=\frac{1}{2}}_{N^*,\Sigma K^*}$ and $g_{N^*,\Sigma^0K^{*+}} = -\sqrt{1/3}\, g^{I=\frac{1}{2}}_{N^*,\Sigma K^*}$.

The vertices $K^{*0} \to K^+\pi^-$ and $K^{*+} \to K^+\pi^0$ are calculated by using Eq. (13), which gives

$$-it_{K^{*0},K^+\pi^-} = ig(\vec{q} + 2\vec{k}) \cdot \vec{\epsilon}_{K^*}, \tag{39a}$$

$$-it_{K^{*+},K^+\pi^0} = i\frac{g}{\sqrt{2}}(\vec{q} + 2\vec{k}) \cdot \vec{\epsilon}_{K^*}. \tag{39b}$$

To calculate the cross section for the diagrams in Fig. 4, we proceed as done in Ref. [77]. In Fig. 3, the t matrix found in Eq. (35) is given by

$$t_{ab\to 123} = C' \frac{1}{M_{\rm inv} - M_R + i\frac{\Gamma_R}{2}} g_{R,23}, \tag{40}$$

with C' being a parameter that carries the dependence of the amplitude on the variable t as well as information about the $pp \to pR$ transition. Substituting

$$\Gamma_{R,23} = \frac{1}{2\pi}\frac{M_3}{M_{\rm inv}} g_{R,23}^2 |\vec{\tilde{p}}_2|, \tag{41}$$

where particle 3 is assumed to be a baryon, into Eq. (35), we get

$$\frac{d^2\sigma}{dt dM_{\rm inv}} = \frac{\prod_F (2M_F)}{32 p_a^2 s (2\pi)^3} |C'|^2 \left|\frac{1}{M_{\rm inv} - M_R + i\frac{\Gamma_R}{2}}\right|^2 \times 2\pi \frac{M_{\rm inv}}{M_3}\Gamma_{R,23}. \tag{42}$$

Now we can take into account the complete reaction by substituting $\Gamma_{R,23}$ for $\Gamma_{N^*\to K^+\pi\Sigma}$, where

$$\frac{d\Gamma_{N^*\to K^+\pi\Sigma}}{dm_{\rm inv}} = \frac{2M_{N^*}2M_\Sigma}{(2\pi)^3 4M_{\rm inv}^2} |\vec{p}_K||\vec{\tilde{p}}_\pi| \overline{\sum} \sum |t'|^2, \tag{43}$$

with $|\vec{p}_K|$ being the momentum of K in the rest frame of N^*,

$$|\vec{p}_K| = \frac{\lambda^{\frac{1}{2}}\left(M_{\rm inv}^2, m_K^2, m_{\rm inv}^2\right)}{2M_{\rm inv}}, \tag{44}$$

and $|\vec{\tilde{p}}_\pi|$ is the π momentum in the $\pi\Sigma$ c.m. given by Eq. (4).

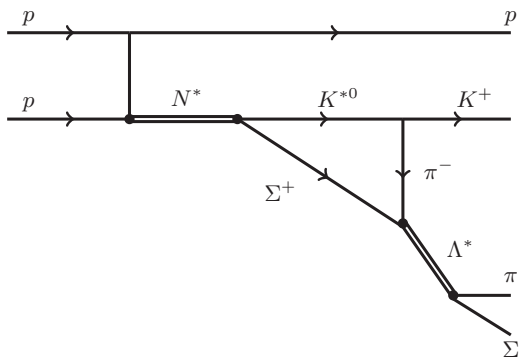

(a)

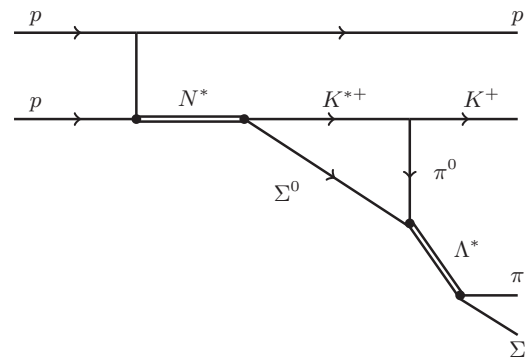

(b)

FIG. 4. Diagrams for reaction $pp \to pK^+\pi\Sigma$ that contains the triangle mechanism, where $\pi\Sigma$ can be $\pi^-\Sigma^+$, $\pi^0\Sigma^0$, or $\pi^+\Sigma^-$.

Then, from Eq. (42) we obtain

$$\frac{d^3\sigma_{pK^+\pi\Sigma}}{dt\, dM_{\rm inv} dm_{\rm inv}} = \frac{(2M_p)^3\, 2M_\Sigma}{32 p_a^2 s (2\pi)^5} |\vec{p}_K||\vec{\tilde{p}}_\pi||C'|^2 \times \left| \frac{1}{M_{\rm inv} - M_{N^*} + i\frac{\Gamma_{N^*}}{2}} \right|^2 \overline{\sum} \sum |t'|^2. \tag{45}$$

The transition amplitude t' in Eq. (45) is

$$t' = \sqrt{\frac{2}{3}} 2M_\Sigma g^{I=\frac{1}{2}}_{N^*,\Sigma K^*} g \left(t_{\Sigma^+\pi^-,\Sigma\pi} + \frac{1}{2} t_{\Sigma^0\pi^0,\Sigma\pi} \right) \vec{\sigma}\cdot\vec{k} t_T, \tag{46}$$

which is constructed in a way similar to what was done in the previous section to obtain Eq. (28) but now changing the following variables in Eq. (26):

$$P^0 = M_{\rm inv}, \tag{47a}$$

$$|\vec{k}| = |\vec{p}_K| = \frac{\lambda^{\frac{1}{2}}(M^2_{\rm inv}, m^2_K, m^2_{\rm inv})}{2M_{\rm inv}}, \tag{47b}$$

$$k^0 = \frac{M^2_{\rm inv} + m^2_K - m^2_{\rm inv}}{2M_{\rm inv}}. \tag{47c}$$

Putting Eq. (46) into Eq. (45), we get

$$\frac{d^3\sigma_{pK^+\pi\Sigma}}{dt\, dM_{\rm inv} dm_{\rm inv}} = C'' \frac{1}{\left|M_{\rm inv} - M_{N^*} + i\frac{\Gamma_{N^*}}{2}\right|^2} |\vec{\tilde{p}}_\pi| \left| t_{\Sigma^+\pi^-,\Sigma\pi} + \frac{1}{2} t_{\Sigma^0\pi^0,\Sigma\pi} \right|^2 |\vec{k}|^3 |t_T|^2, \tag{48}$$

where $|\vec{\tilde{p}}_\pi|$ is the π momentum in the $\pi\Sigma$ c.m.,

$$|\vec{\tilde{p}}_\pi| = \frac{\lambda^{\frac{1}{2}}(m^2_{\rm inv}, m^2_\pi, M^2_\Sigma)}{2m_{\rm inv}}, \tag{49}$$

and

$$C'' = \frac{2}{3} \frac{(2M_p)^3\, 2M_\Sigma}{32 p_a^2 s (2\pi)^5} \left| g^{I=\frac{1}{2}}_{N^*,\Sigma K^*} \right|^2 g^2 (2M_\Sigma)^2 |C'|^2, \tag{50}$$

which is a function of $s = (p_a + p_b)^2$ and $t = (p_a - p_1)^2$.

Using now the relation

$$dt = 2|\vec{p}_a||\vec{p}_1|\, d\cos\theta, \tag{51}$$

which follows from $t = (p_a - p_1)^2$, we then obtain

$$\frac{d^3\sigma_{pK^+\pi\Sigma}}{d\cos\theta\, dM_{\rm inv} dm_{\rm inv}} = C'' \frac{2|\vec{p}_a||\vec{p}_1|}{\left|M_{\rm inv} - M_{N^*} + i\frac{\Gamma_{N^*}}{2}\right|^2} |\vec{\tilde{p}}_\pi| \left| t_{\Sigma^+\pi^-,\Sigma\pi} + \frac{1}{2} t_{\Sigma^0\pi^0,\Sigma\pi} \right|^2 |\vec{k}|^3 |t_T|^2, \tag{52}$$

with

$$|\vec{p}_a| = \frac{\lambda^{\frac{1}{2}}(s, M_p^2, M_p^2)}{2\sqrt{s}}, \tag{53a}$$

$$|\vec{p}_1| = \frac{\lambda^{\frac{1}{2}}(s, M_p^2, M^2_{\rm inv})}{2\sqrt{s}}. \tag{53b}$$

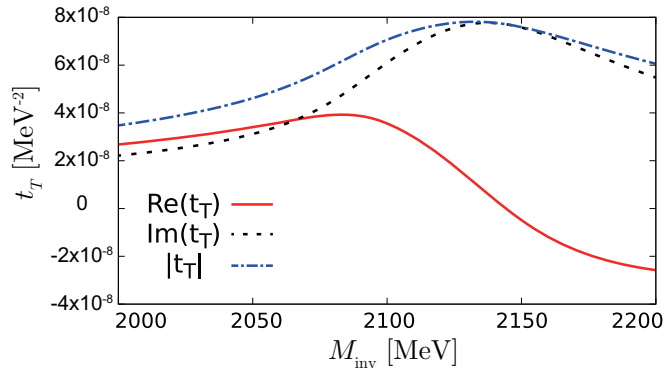

FIG. 5. $\mathrm{Re}(t_T)$, $\mathrm{Im}(t_T)$, and $|t_T|$ of Eq. (26).

This last step is important to account for the phase space of this process that depends on $|\vec{p}_1|$, which is tied to $M_{\rm inv}$.

Finally, we should integrate out the $\cos\theta$ in Eq. (52) but C' in C'' depend on it. The resultant factor of the $\cos\theta$ integration is denoted by C''' and since we do not know the expression for C', we take $C''' = 1$. This means that from now on we will use arbitrary units (arb. unit) for the cross section.

Thus, we end up with

$$\frac{d^2\sigma_{pK^+\pi\Sigma}}{dM_{\rm inv} dm_{\rm inv}} = \frac{C'''2|\vec{p}_a||\vec{p}_1|}{\left|M_{\rm inv} - M_{N^*} + i\frac{\Gamma_{N^*}}{2}\right|^2} |\vec{\tilde{p}}_\pi| \left| t_{\Sigma^+\pi^-,\Sigma\pi} + \frac{1}{2} t_{\Sigma^0\pi^0,\Sigma\pi} \right|^2 |\vec{k}|^3 |t_T|^2. \tag{54}$$

III. RESULTS

In Fig. 5, we show the real part, imaginary part, and absolute value of the amplitude t_T of Eq. (26) as a function of the invariant mass of $K\Lambda(1405)$, $M_{\rm inv}$, by fixing the invariant mass of $\pi\Sigma$, $m_{\rm inv}$, at 1400 MeV. The absolute value of t_T has a peak around 2140 MeV as expected from the condition for a triangular singularity by Eq. (18) of Ref. [53], and the peak is dominated by the imaginary part of the amplitude. As mentioned in Ref. [56], the peak of the imaginary part is responsible for the triangle singularity.

In Fig. 6, we plot the mass distribution of the $\pi^- p \to K^0\pi\Sigma$ scattering process as a function of $m_{\rm inv}(\pi^0\Sigma^0)$, $m_{\rm inv}(\pi^+\Sigma^-)$, and $m_{\rm inv}(\pi^-\Sigma^+)$ with a fixed $\sqrt{s} = M_{\rm inv}$=2050, 2100, 2140, 2200, 2230 MeV. Let us first look at the $\pi^0\Sigma^0$ mass distribution in Fig. 6. At $M_{\rm inv} = 2140$ MeV, where a peak associated with the triangle singularity is expected from the formula in Ref. [53], we can see a clear peak at 1400 MeV associated with $\Lambda(1405)$ in the $\pi\Sigma$ invariant mass. As we see in the figure the largest strength is obtained with $M_{\rm inv} =$ 2100 MeV. A peak is found around 1385 MeV for $M_{\rm inv} =$ 2200,2230 MeV with a smaller strength, and the peak position moves toward higher energy a little for $M_{\rm inv} = 2050$ MeV. In the case of the $\pi^+\Sigma^-$ and $\pi^-\Sigma^+$ final states, while the basic features are shared with $\pi^0\Sigma^0$, the peak positions of the the $\pi^+\Sigma^-$ mass distribution are about 5 MeV less than that of the $\pi^0\Sigma^0$ mass distribution, and the peak positions in the $\pi^-\Sigma^+$ mass distribution are about 5 MeV bigger than the values of the $\pi^0\Sigma^0$ mass distribution with a similar width and strength.

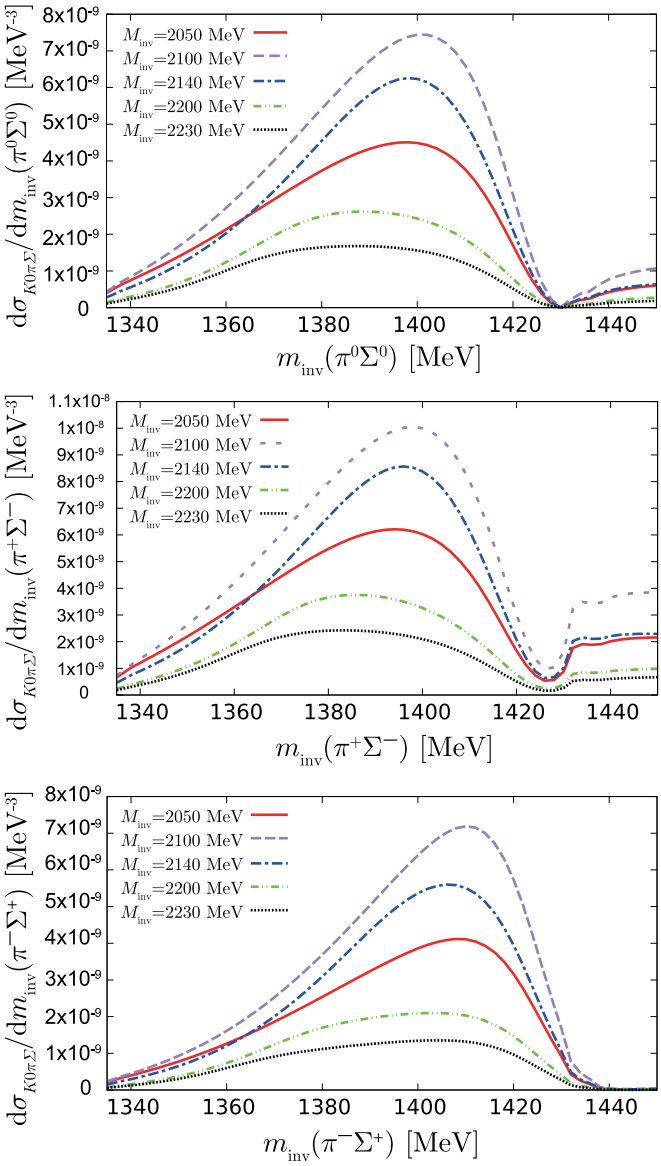

FIG. 6. The $d\sigma/dm_{\rm inv}$ mass distribution as a function of $m_{\rm inv}(\pi^0\Sigma^0)$, $m_{\rm inv}(\pi^+\Sigma^-)$, and $m_{\rm inv}(\pi^-\Sigma^+)$ for the $\pi^- p \to K^0\pi\Sigma$ scattering with several fixed values of $M_{\rm inv}$.

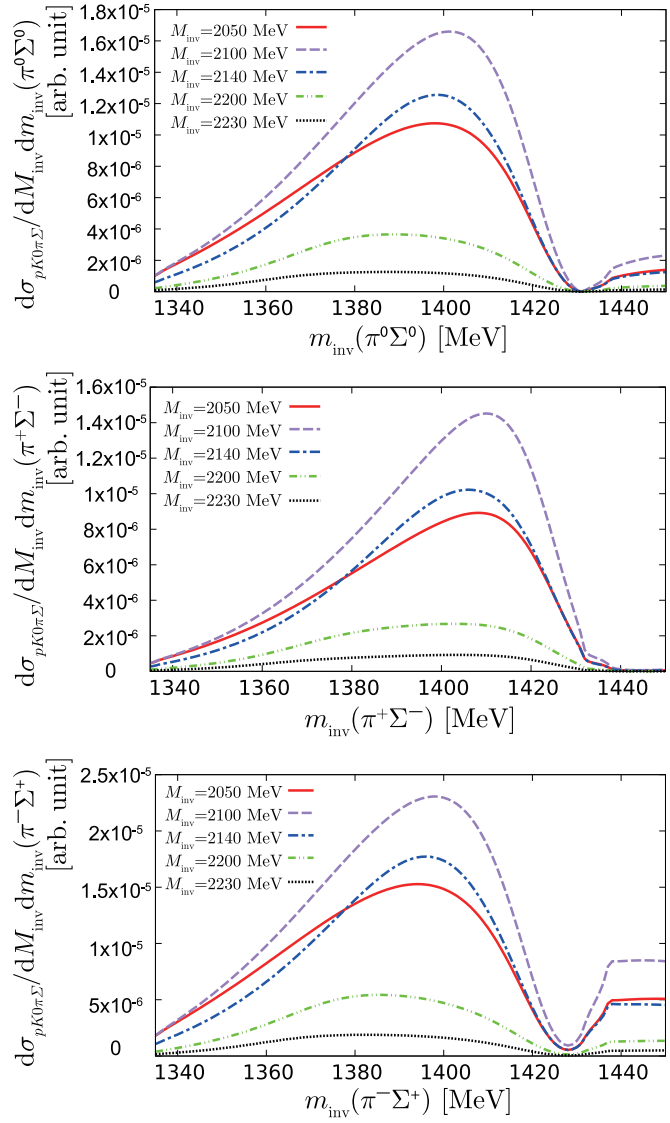

FIG. 7. The $d^2\sigma_{pK^+\pi\Sigma}/dM_{\rm inv}dm_{\rm inv}$ as a function of $m_{\rm inv}(\pi^0\Sigma^0)$, $m_{\rm inv}(\pi^+\Sigma^-)$, and $m_{\rm inv}(\pi^-\Sigma^+)$ for the $pp \to pK^+\pi\Sigma$ scattering with several fixed values of $M_{\rm inv}$ and $\sqrt{s} = 3179$ MeV.

Among these processes, the $\pi^+\Sigma^-$ gives the largest strength. This is roughly because the $t_{\Sigma^-\pi^+,\Sigma\pi}$ term is twice as larger as $t_{\Sigma^0\pi^0,\Sigma\pi}$ in Eq. (30).

As stated before Eq. (7), we separate the $\pi^0\Sigma^0$, $\pi^+\Sigma^-$, and $\pi^-\Sigma^+$ channels, although an isospin formalism could be equally implemented. Indeed, N^* has $I = 1/2$ and thus the final $K\pi\Sigma$ state also has $I = 1/2$, but the $\pi\Sigma$ subsystem can be either $I = 0$ or $I = 1$, and the amplitudes $\pi\Sigma \to \pi\Sigma$ have a contribution of both $I = 0$ and $I = 1$ and even a small one of $I = 2$, and these contributions appear with different signs in the charge channels, thus leading to different mass distributions. These differences between cross sections of the $\pi\Sigma$ channels were predicted in the theoretical study of the $\gamma p \to K^+\pi\Sigma$ reaction in Ref. [24] and corroborated by experiments done in Refs. [80,81].

In Fig. 7, we show the results of $d^2\sigma_{pK^+\pi\Sigma}/dM_{\rm inv}dm_{\rm inv}$ for the $pp \to pK^+\pi\Sigma$ scattering as a functions of $m_{\rm inv}(\pi^0\Sigma^0)$, $m_{\rm inv}(\pi^+\Sigma^-)$, and $m_{\rm inv}(\pi^-\Sigma^+)$, respectively. The total energy of the system $\sqrt{s}$ is fixed at 3179 MeV which can be accessed experimentally [64–66]. The dependence on $m_{\rm inv}$ is similar to that in $d\sigma_{K^0\pi\Sigma}/dm_{\rm inv}$. In the case of $\pi^0\Sigma^0$ the peak is located at 1400 MeV by fixing $M_{\rm inv} = 2140$ MeV. For $M_{\rm inv} = 2200$ and 2230 MeV, the peak positions move towards 1380 MeV and also the widths are broader than that of the 1400 MeV case. Decreasing the value of $M_{\rm inv}$ to 2100 MeV, we obtain the peak position around 1405 MeV. The shape of results are similar for the $\pi^+\Sigma^-$ and $\pi^-\Sigma^+$ mass distributions, but the peak positions are 10 MeV bigger for the case of $\pi^+\Sigma^-$ and 5 MeV smaller for $\pi^-\Sigma^+$ mass distribution. In these processes, $\pi^-\Sigma^+$ gives the largest strength because of the additional factor two for the $t_{\Sigma^+\pi^-,\Sigma\pi}$ term in Eq. (52) compared with $t_{\Sigma^0\pi^0,\Sigma\pi}$. We should note that the peak with this mechanism appears at lower $\pi\Sigma$

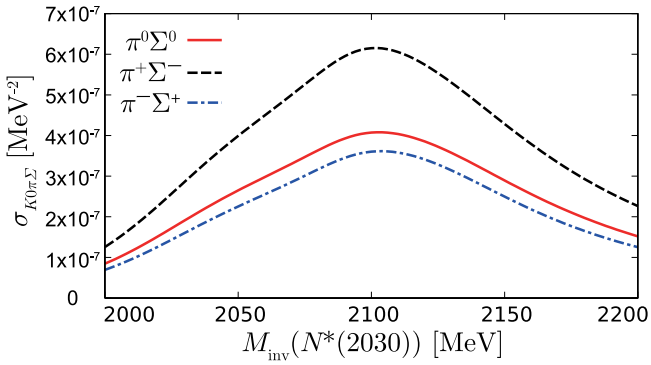

FIG. 8. Cross section of $\pi^- p \to K^0\pi\Sigma$ process $\sigma_{K^0\pi\Sigma}$ as a function of $M_{\rm inv}$ for $\pi^- p \to K^0\pi\Sigma$ scattering. The red solid line corresponds to $\pi^0\Sigma^0$, the black dash line corresponds to $\pi^+\Sigma^-$, and the blue dash-dotted line corresponds to $\pi^-\Sigma^+$.

invariant mass than with the model of Ref. [36], where the peak showed at 1420 MeV. This is due to the fact that with the TS, $\Lambda(1405)$ is formed by $\pi\Sigma$, rather than by $\bar{K}N$, and this channel couples mostly to the lower-mass state of the two $\Lambda(1405)$ states [10].

For the case of the $\pi^- p \to K^0\pi\Sigma$ reaction, we integrate $d\sigma_{K^0\pi\Sigma}/dm_{\rm inv}$ over $m_{\rm inv}$ in the range of the $\Lambda(1405)$ peak, $m_{\rm inv} \in (m_\pi + m_\Sigma, 1450$ MeV), where m_π and m_Σ are the isospin-averaged mass of π and Σ, and we obtain the cross section of $\pi^- p \to K^0\pi\Sigma$ and $\sigma_{K^0\pi\Sigma}$ as a function of $M_{\rm inv}$. The results are represented in Fig. 8. There are peaks around 2100 MeV for all cases, although the expected value of triangular singularity is 2140 MeV. This is because the N^* resonance in the $K^*\Sigma$ production has a peak around 2030 MeV [the term $1/|M_{\rm inv} - M_{N^*} + i\frac{\Gamma_{N^*}}{2}|^2$ in Eq. (52)].

For the case of the $pp \to pK^+\pi\Sigma$ reaction, integrating now the $d^2\sigma_{pK^+\pi\Sigma}/dM_{\rm inv}dm_{\rm inv}$ over $m_{\rm inv}$ we obtain $d\sigma_{pK^+\pi\Sigma}/dM_{\rm inv}$ which is shown in Fig. 9 as a function of

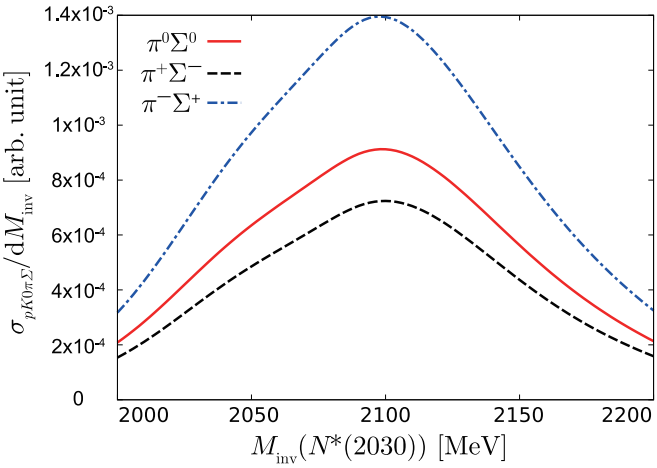

FIG. 9. $d\sigma_{pK^+\pi\Sigma}/dM_{\rm inv}$ as a function of $M_{\rm inv}$ for $pp \to pK^+\pi\Sigma$ scattering with fixed value of $\sqrt{s} = 3179$ MeV. The red solid line corresponds to $\pi^0\Sigma^0$, the black dash line corresponds to $\pi^+\Sigma^-$, and the blue dash-dotted line corresponds to $\pi^-\Sigma^+$.

$M_{\rm inv}$ for $\pi^0\Sigma^0$, $\pi^+\Sigma^-$, and $\pi^-\Sigma^+$. Similarly, we get peaks around 2100 MeV for the three cases.

In the $\pi^- p$ and pp reactions, the strength is largest for the $\pi^+\Sigma^-$ and $\pi^-\Sigma^+$ final state, respectively, reflecting the strength before the integration shown in Figs. 6 and 7.

We should note that the $N^*(2030)$ is about 50 MeV below the $K^*\Sigma$ threshold, but the width of about 125 MeV makes the overlap of the resonance in the region of $K^*\Sigma$ invariant masses studied still sizable, and the important thing is that this resonance has a large coupling to the $K^*\Sigma$ channel as we have discussed. We can also rightly question whether the structure found for t_T is not tied to two-body thresholds rather than to the TS. We can have two thresholds where (in the absence of a K^* width) two singularities (finite) would appear: the $K^*\Sigma$ threshold and the $\Sigma\pi$ threshold. The latter one appears at 1337 MeV but the peaks in the $\pi\Sigma$ mass distributions show up at about 1400 MeV, related to $\Lambda(1405)$, thus it is not the $\pi\Sigma$ threshold enhancement that one is seeing there. The $K^*\Sigma$ threshold appears at 2087 MeV, and the width of the K^* softens a structure related to this threshold. Actually, we see a soft enhancement of Re(t_T) in Fig. 5 around this energy. This is related to this threshold and a detailed study of the threshold effect and the TS, going to the limit of small width, was conducted in Ref. [56] where a triangle diagram with K^*DK intermediate states was studied. It was indeed found that Re(t_T) had a bump associated with the K^*D threshold while Im(t_T) had a peak stemming from a triangle singularity. Here we have a similar situation where Re(t_T) in Fig. 5 is influenced by the $K^*\Sigma$ threshold, while Im(t_T) is driven by the TS peaking at higher energy. We see in Fig. 5, by looking at $|t_T|$, that the peak structure is just provided by Im(t_T), so it is the TS that is responsible for the peak structure in the cross sections studied.

We note that our calculations are done without a normalization. In the case of the $\pi^- p \to K^0\pi\Sigma$ reaction we made an estimate of the absolute value by assuming a $N^*(2030)$ decay width to πN of about 70 MeV. This is only a guess of the order of magnitude based on similar decay widths for N^* resonances in that energy range. It is not possible right now to be more quantitative. In the case of the $pp \to pK^+\pi\Sigma$ reaction, we did not even attempt to make an estimate of the absolute value of the cross section. Yet, the results that we find in the next section, where we show that the triangle mechanism is far more important than the tree-level diagram, give us confidence that the triangle mechanism discussed here is indeed very important and provides a plausible solution to the puzzle of the experimental results of Ref. [65]. At present we would suggest that an experimental exploration is done of the dependence of the cross sections on the $K^+\pi\Sigma$ invariant mass to see if the predictions tied to the TS studied here hold. A further theoretical study after some extra experimental information from these observables would then be advisable.

IV. FURTHER CONSIDERATIONS

The paper has relied on a triangle loop with $K^*\pi\Sigma$ in the intermediate state. We can ask what happens to the related tree-level mechanism with the same final state. Then we can consider the mechanism of Fig. 10 for the $pp \to pK^+\pi^-\Sigma^+$ reaction. The first thing we realize is that, in this mechanism,

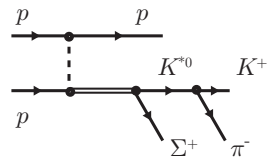

FIG. 10. Tree-level diagram corresponding to Fig. 4(a) with the fixed $\pi\Sigma$ being $\pi^-\Sigma^+$.

$\pi^+\Sigma^-$ are not in a resonant state [the $\Lambda(1405)$] unlike in Fig. 4(a). Its contribution will appear as a background that in experiments is removed to get the $\Lambda(1405)$ signal. Yet we can make an estimate of this contribution relative to the loop mechanism of Fig. 4. We must replace in Eq. (54)

$$2M_\Sigma\left(t_{\Sigma^+\pi^-,\Sigma^+\pi^-}+\tfrac{1}{2}t_{\Sigma^0\pi^0,\Sigma^+\pi^-}\right)\vec{\sigma}\cdot\vec{k}\,t_T \tag{55}$$

by

$$\frac{1}{M^2_{\rm inv}(\pi^-K^+)-m^2_{K^*}+im_{K^*}\Gamma_{K^*}}\vec{\sigma}\cdot(\vec{k}-\vec{p}_\pi). \tag{56}$$

We have made estimates of these two terms in the region of the peak of $M_{\rm inv}(K^{*0}\Sigma^+)$ ($\sim$2100 MeV) and of the peak of $M_{\rm inv}(\pi^-\Sigma^+)$ ($\sim$1400 MeV) and we find the tree level small compared with the loop terms, of the order of five times smaller, and out of phase with the other mechanism, which gives rise to a small background below the structure that we have studied.

Next we would like to see what happens if we had a mechanism with $\bar{K}N$ instead of $\pi\Sigma$ in the loop. Our argumentation is that, by having $\pi\Sigma$ in the loop we guarantee that the $\Lambda(1405)$ state of small energy (1385–1400 MeV) is produced. However, should there be a mechanism with $\bar{K}N$ in the loop, then the $\Lambda(1405)$ state of higher energies ($\sim$1420 MeV) would be produced and we would reach different conclusions in the paper. Actually, related to the mechanism that we have, we could have the mechanism of Fig. 11. The same resonance N^* that we have discussed also couples to ϕN. However, as we can see in Fig. 2 of Ref. [60] the strength of the N^* resonance coupling to the ϕN channel is of the order of 0.25 compared with 7 for the coupling to $K^*\Sigma$ that we have considered here. This is about a factor 30 smaller than the mechanism we have considered.

We can also see at which $M_{\rm inv}(\phi n)$ value one expects the triangle singularity peak, and we find it at $M_{\rm inv}(\phi n)=1970$ MeV [we put the mass of $\Lambda(1405)$ as 1433 MeV to be above the $\bar{K}N$ threshold and to be able to apply Eq. (18) of Ref. [53]]. This energy is lower than the energy of 2100 MeV where the former triangle singularity appeared. This invariant mass is lower than the one reached in the $\pi^-p\to K^0\pi\Sigma$ experiments of Refs. [62,63]. It is at reach in the $pp\to pK^+\pi\Sigma$ experiment

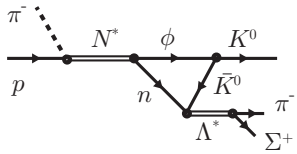

FIG. 11. Triangle mechanism with $\phi n\bar{K}^0$ intermediate state.

of Ref. [65]. In addition, the small width of the ϕ makes the TS structure narrower, but the p-wave coupling of $\phi\to K\bar{K}$ reduces drastically the strength. Indeed, the $|\vec{k}\,|^3$ factor in the cross sections of Eqs. (1) and (30) for $\pi^-p\to K^0\pi\Sigma$ and Eq. (54) for $pp\to pK^+\pi\Sigma$ introduces an extra 0.08 relative reduction factor of the $\bar{K}N$ triangle mechanism versus the $K^*\Sigma$ one. The two factors discussed make the $\phi\bar{K}N$ mechanism negligible versus the $K^*\pi\Sigma$ mechanism.

On the other hand, one may wonder if there are other N^* resonances around the 2000–2150 MeV that couple strongly to ϕN, but by looking into the PDG [41] and the older version of the PDG [68], we do not find any resonance with coupling to ϕN.

We could think of other possible vector mesons and N^*. The next vector meson is $\rho(1450)$. This mechanism develops a TS at 2614 MeV [the mass of $\Lambda(1405)$ is again put as 1433 MeV here], which cannot be reached in the experiment of Ref. [65]. In addition, $\rho(1450)\to K\bar{K}$ is quoted as "not seen" in the PDG [41] although some searches are quoted there. Furthermore, we do not know of any N^* resonance around this energy that could have a sizable coupling to $N\rho(1450)$.

Finally, we would like to insist that we have not determined the strength of the cross section. For reasons discussed at the beginning we would need information, the πN decay of N^*, which is not known, and we did estimates. For the case of the pp reaction we simply give results in arbitrary units. However, the comparison done with the tree level, showing that the strength of the triangle mechanism is much more important than the tree level, indicates that the mechanism discussed is relevant for the reaction. Leaving this apart, the shape of the invariant-mass distributions is totally given by the mass and width of the particles in the triangle diagram and there is no uncertainty in the shape.

The discussion above is illustrative and shows the relevant role of the TS with the $K^*\Sigma\pi$ intermediate state, which enhances the excitation of the low-energy $\Lambda(1405)$ state, providing a plausible explanation of the experimental findings of Ref. [65].

V. SUMMARY

We have carried out a study of contributions of a triangle diagram to the the $\pi^-p\to K^0\pi\Sigma$ and $pp\to pK^+\pi\Sigma$ processes. In both reactions, the triangle diagram is formed by N^* decaying first to K^* and Σ, K^* decaying into πK, and then Σ and π merging to give $\Lambda(1405)$, which finally decays into $\pi\Sigma$. In this process, the $K^*\pi\Sigma$ loop generates a triangle singularity around 2140 MeV in the invariant mass of $K\Lambda(1405)$ from Eq. (18) of Ref. [53]. We evaluate the real part, the imaginary part, and the absolute value of the amplitude t_T and find a peak around 2140 MeV. We calculate $d\sigma_{K^0\pi\Sigma}/dm_{\rm inv}$ with some values of $M_{\rm inv}$ in the $\pi^-p\to K^0\pi\Sigma$ reaction and $d^2\sigma_{pK^+\pi\Sigma}/dM_{\rm inv}dm_{\rm inv}$ with some values of $M_{\rm inv}$ and fixed $\sqrt{s}=3179$ MeV as a function of $m_{\rm inv}(\pi^0\Sigma^0)$, $m_{\rm inv}(\pi^+\Sigma^-)$, and $m_{\rm inv}(\pi^-\Sigma^+)$. In these distributions, we see peaks around 1400 MeV, representing clearly $\Lambda(1405)$. Integrating over $m_{\rm inv}$, we obtain $\sigma_{K^0\pi\Sigma}$ and $d\sigma_{pK^+\pi\Sigma}/dM_{\rm inv}$, and these distributions show a clear peak for $M_{\rm inv}(N^*(2030))$ around 2100 MeV. The peak of the singularity shows up around

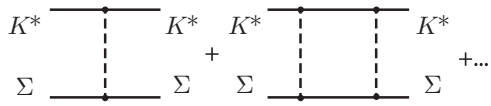

FIG. 12. Source of $K^*\Sigma \to K^*\Sigma$ interaction through vector exchange.

2140 MeV. This peak position of the triangular singularity is lowered by the initial N^* resonance peak around 2030 MeV in the $K^*\Sigma$ production.

Thus, our results constitute an interesting prediction of the triangle singularity effect in the cross sections of these decays. The work done here could explain why in the experiments of Refs. [65,66] the invariant-mass distribution of $\pi\Sigma$ for $\Lambda(1405)$ are found at lower invariant masses than in other reactions. It would also be interesting to see if the predictions done here concerning the triangle singularity are fulfilled by the experimental data, an issue that has not been investigated so far. This work also can serve as a warning to future experiments that measure these interactions that they should be careful when associating peaks in this energy region to resonances.

ACKNOWLEDGMENTS

R.P. Pavao wishes to thank the Generalitat Valenciana in the program Santiago Grisolia. This work was partly supported by the Spanish Ministerio de Economia y Competitividad and European FEDER funds under the Contracts No. FIS2014-57026-REDT, No. FIS2014-51948-C2-1-P, and No. FIS2014-51948-C2-2-P, and the Generalitat Valenciana in the program Prometeo II-2014/068.

APPENDIX: SPIN 1/2 AND 3/2 CONTRIBUTION

For $K^*\Sigma \to K^*\Sigma$, we have the contribution from vector exchange in Ref. [60] as shown in Fig. 12. The contribution close to the resonance pole is given by

$$t_{K^*\Sigma,K^*\Sigma} = \frac{g^2_{K^*\Sigma}}{\sqrt{s} - M_R + i\Gamma_R/2}\vec{\epsilon}\cdot\vec{\epsilon}\,' \equiv t_R\vec{\epsilon}\cdot\vec{\epsilon}\,', \tag{A1}$$

where $\vec{\epsilon}$ and $\vec{\epsilon}\,'$ are the polarization vectors of the initial and final vectors. This amplitude contains both spin 1/2 and 3/2. It is easy to split this into spin 1/2 and 3/2. We can write symbolically the amplitude of Fig. 12 as in Fig. 13. We can write the vertices corresponding to Fig. 14 as

$$\tilde{t}^{\,(1/2)}_{K^*\Sigma} = \frac{1}{\sqrt{3}} g_{K^*\Sigma}\vec{\sigma}\cdot\vec{\epsilon}, \tag{A2}$$

$$\tilde{t}^{\,(3/2)}_{K^*\Sigma} = g_{K^*\Sigma}\vec{S}\cdot\vec{\epsilon}, \tag{A3}$$

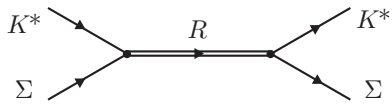

FIG. 13. Representation of Fig. 12 in terms of the resonance generated by the mechanism of Fig. 12.

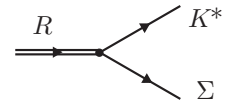

FIG. 14. Effective $R \to K^*\Sigma$ vertex.

where $\vec{S}$ is the transition operator from spin 3/2 to 1/2, with the properties

$$\sum_{m_s} \sigma_i|m_s\rangle\langle m_s|\sigma_j = \delta_{ij} + i\epsilon_{ijk}\sigma_k, \tag{A4}$$

$$\sum_{M_s} S_i|M_s\rangle\langle M_s|S_j^\dagger = \frac{2}{3}\delta_{ij} - \frac{i}{3}\epsilon_{ijk}\sigma_k. \tag{A5}$$

Each of these operators projects the amplitude of Fig. 13 over spin 1/2 and 3/2, respectively, and we have

$$\begin{aligned} t_R^{(1/2+3/2)} &= t_R\left\{\tfrac{1}{3}\vec{\sigma}\cdot\vec{\epsilon}\;\vec{\sigma}\cdot\vec{\epsilon}\,' + \vec{S}\cdot\vec{\epsilon}\;\vec{S}^\dagger\cdot\vec{\epsilon}\,'\right\} \\ &= t_R\vec{\epsilon}\cdot\vec{\epsilon}\,', \end{aligned} \tag{A6}$$

which gives us the proper separation of the amplitude of Fig. 13 into its spin 1/2 and 3/2 parts. By using the vertices of Eqs. (A2) and (A3) it is easy to see that

$$\overline{\sum}\sum|\tilde{t}^{\,(1/2)}_{K^*\Sigma}|^2 = \overline{\sum}\sum|\tilde{t}^{\,(3/2)}_{K^*\Sigma}|^2 = g^2_{K^*\Sigma}, \tag{A7}$$

which means that, by using the form of Eq. (A1), one has the same width of $R \to K^*\Sigma$ for $J = 1/2$ and $J = 3/2$ and one can use the coupling $g_{K^*\Sigma}$ for either case, ignoring the spin variables, as done in Ref. [60].

The coupling to πN proceeds via the loop shown in Fig. 15 [60,67]. We are only concerned about the ratio between $J = 1/2$ and 3/2, so we assume that the loop of Fig. 15 is dominated by the on-shell intermediate $K^*\Sigma$. In the limit of small K^* momentum and separating the product of the $K^* \to K\pi$ and $\Sigma K \to N$ vertices into S and D waves [we remove the factor of 2 from $\vec{\epsilon}\cdot(\vec{p}_\pi - \vec{p}_K) = 2\vec{\epsilon}\cdot\vec{p}_\pi$ for simplicity], we find

$$\vec{\epsilon}\cdot\vec{p}_\pi\;\vec{\sigma}\cdot\vec{p}_\pi = \epsilon_i\sigma_j\frac{|\vec{p}_\pi|^2}{3}\delta_{ij} + \epsilon_i\sigma_j\left(p_{\pi i}p_{\pi j} - \frac{|\vec{p}_\pi|^2}{3}\delta_{ij}\right), \tag{A8}$$

the couplings of the πN to N^* with $J = 1/2$ and 3/2 are given by

$$\begin{aligned} \tilde{t}^{\,(1/2)}_{\pi N} &= \sum_{K^*\text{ pol.}}\frac{\tilde{g}}{3}|\vec{p}_\pi|^2\vec{\sigma}\cdot\vec{\epsilon}\,\frac{g_{K^*\Sigma}}{\sqrt{3}}\vec{\sigma}\cdot\vec{\epsilon} = \frac{\tilde{g}g_{K^*\Sigma}}{3\sqrt{3}}|\vec{p}_\pi|^2\vec{\sigma}\cdot\vec{\sigma} \\ &= \frac{1}{\sqrt{3}}\tilde{g}g_{K^*\Sigma}|\vec{p}_\pi|^2 \quad \text{for } J = 1/2, \end{aligned} \tag{A9}$$

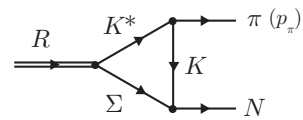

FIG. 15. Effective mechanism for $R \to \pi N$.

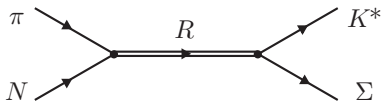

FIG. 16. Mechanism for $\pi N \to K^*\Sigma$ combining the vertices of Figs. 13 and 15.

$$\tilde{t}^{(3/2)}_{\pi N} = \sum_{K^* \text{ pol.}} \tilde{g}\epsilon_i\sigma_j\left(p_{\pi i}p_{\pi j} - \frac{1}{3}|\vec{p}_\pi|^2\delta_{ij}\right) g_{K^*\Sigma}\vec{S}\cdot\vec{\epsilon}$$
$$= \tilde{g}g_{K^*\Sigma}\sigma_j S_i\left(p_{\pi i}p_{\pi j} - \frac{1}{3}|\vec{p}_\pi|^2\delta_{ij}\right) \quad \text{for } J = 3/2. \tag{A10}$$

Next, we look at the $\pi N \to K^*\Sigma$ transition of Fig. 16 and we have

$$\bar{t}^{(1/2)}_{\pi N,K^*\Sigma} = \frac{g_{K^*\Sigma}}{\sqrt{3}}\vec{\sigma}\cdot\vec{\epsilon}\,\frac{1}{\sqrt{s} - M_R + i\Gamma_R/2}\,\frac{\tilde{g}g_{K^*\Sigma}}{\sqrt{3}}|\vec{p}_\pi|^2$$
$$\equiv \frac{\tilde{g}}{3}\vec{\sigma}\cdot\vec{\epsilon}\,|\vec{p}_\pi|^2 t_R, \tag{A11}$$

$$\bar{t}^{(3/2)}_{\pi N,K^*\Sigma} = g_{K^*\Sigma}\vec{S}\cdot\vec{\epsilon}\,\frac{1}{\sqrt{s} - M_R + i\Gamma_R/2}$$
$$\times\, \tilde{g}g_{K^*\Sigma}S_i^\dagger\sigma_j\left(p_{\pi i}p_{\pi j} - \frac{1}{3}|\vec{p}_\pi|^2\delta_{ij}\right)$$
$$= \tilde{g}\left(\vec{\sigma}\cdot\vec{p}_\pi\vec{\epsilon}\cdot\vec{p}_\pi - \frac{1}{3}|\vec{p}_\pi|^2\vec{\sigma}\cdot\vec{\epsilon}\right)t_R. \tag{A12}$$

In the coupling $\tilde{g}$ we have included for convenience the result that would come from the loop integration of Fig. 15, which is common to $J = 1/2$ and $J = 3/2$.

We can sum Eqs. (A11) and (A12) to account for both the spin 1/2 and 3/2 (if one adds incoherently the cross sections one obtains the same result, because spin 1/2 and 3/2 do not interfere) and we get

$$\bar{t}^{(1/2+3/2)}_{\pi N,K^*\Sigma} = \tilde{g}\vec{\sigma}\cdot\vec{p}_\pi\vec{\epsilon}\cdot\vec{p}_\pi t_R. \tag{A13}$$

Since in the scattering $\vec{p}_\pi$ is in the z direction we can write

$$\bar{t}^{(1/2+3/2)}_{\pi N,K^*\Sigma} = \tilde{g}|\vec{p}_\pi|^2\sigma_3\epsilon_3 t_R. \tag{A14}$$

In the triangle loop of Fig. 1, $\epsilon_3 \to k_3$ and then we get a factor $\sigma_3 k_3$ instead of $\vec{\sigma}\cdot\vec{k}/3$ by using Eq. (A11) for $J = 1/2$.

[1] N. Isgur and G. Karl, Phys. Rev. D **18**, 4187 (1978).
[2] R. H. Dalitz and S. F. Tuan, Phys. Rev. Lett. **2**, 425 (1959).
[3] R. H. Dalitz and S. F. Tuan, Ann. Phys. (NY) **10**, 307 (1960).
[4] R. H. Dalitz, T. C. Wong, and G. Rajasekaran, Phys. Rev. **153**, 1617 (1967).
[5] N. Kaiser, P. B. Siegel, and W. Weise, Nucl. Phys. A **594**, 325 (1995).
[6] E. Oset and A. Ramos, Nucl. Phys. A **635**, 99 (1998).
[7] J. A. Oller and U.-G. Meissner, Phys. Lett. B **500**, 263 (2001).
[8] M. F. M. Lutz and E. E. Kolomeitsev, Nucl. Phys. A **700**, 193 (2002).
[9] C. Garcia-Recio, J. Nieves, E. R. Arriola, and M. J. Vicente Vacas, Phys. Rev. D **67**, 076009 (2003).
[10] D. Jido, J. A. Oller, E. Oset, A. Ramos, and U.-G. Meissner, Nucl. Phys. A **725**, 181 (2003).
[11] B. Borasoy, R. Nissler, and W. Weise, Eur. Phys. J. A **25**, 79 (2005).
[12] Y. Ikeda, T. Hyodo, D. Jido, H. Kamano, T. Sato, and K. Yazaki, Prog. Theor. Phys. **125**, 1205 (2011).
[13] Y. Ikeda, T. Hyodo, and W. Weise, Nucl. Phys. A **881**, 98 (2012).
[14] Z. H. Guo and J. A. Oller, Phys. Rev. C **87**, 035202 (2013).
[15] A. Feijoo, V. K. Magas, and A. Ramos, Phys. Rev. C **92**, 015206 (2015).
[16] M. Mai and U.-G. Meißner, Eur. Phys. J. A **51**, 30 (2015).
[17] J. M. M. Hall, W. Kamleh, D. B. Leinweber, B. J. Menadue, B. J. Owen, A. W. Thomas, and R. D. Young, Phys. Rev. Lett. **114**, 132002 (2015).
[18] R. Molina and M. Döring, Phys. Rev. D **94**, 056010 (2016); **94**, 079901 (2016).
[19] T. Sekihara, T. Hyodo, and D. Jido, PTEP **2015**, 063D04 (2015).
[20] Z. H. Guo and J. A. Oller, Phys. Rev. D **93**, 096001 (2016).
[21] Y. Kamiya and T. Hyodo, Phys. Rev. C **93**, 035203 (2016).
[22] T. Sekihara, T. Hyodo, and D. Jido, Phys. Lett. B **669**, 133 (2008).
[23] K. Miyahara and T. Hyodo, Phys. Rev. C **93**, 015201 (2016).
[24] J. C. Nacher, E. Oset, H. Toki, and A. Ramos, Phys. Lett. B **455**, 55 (1999).
[25] J. C. Nacher, E. Oset, H. Toki, and A. Ramos, Phys. Lett. B **461**, 299 (1999).
[26] B. Borasoy, P. C. Bruns, U.-G. Meissner, and R. Nissler, Eur. Phys. J. A **34**, 161 (2007).
[27] L. Roca and E. Oset, Phys. Rev. C **87**, 055201 (2013).
[28] S. X. Nakamura and D. Jido, PTEP **2014**, 023D01 (2014).
[29] E. Wang, J. J. Xie, W. H. Liang, F. K. Guo, and E. Oset, Phys. Rev. C **95**, 015205 (2017).
[30] V. K. Magas, E. Oset, and A. Ramos, Phys. Rev. Lett. **95**, 052301 (2005).
[31] T. Hyodo, A. Hosaka, E. Oset, A. Ramos, and M. J. Vicente Vacas, Phys. Rev. C **68**, 065203 (2003).
[32] D. Jido, E. Oset, and T. Sekihara, Eur. Phys. J. A **42**, 257 (2009).
[33] K. Miyagawa and J. Haidenbauer, Phys. Rev. C **85**, 065201 (2012).
[34] D. Jido, E. Oset, and T. Sekihara, Eur. Phys. J. A **49**, 95 (2013).
[35] S. Ohnishi, Y. Ikeda, T. Hyodo, and W. Weise, Phys. Rev. C **93**, 025207 (2016).
[36] L. S. Geng and E. Oset, Eur. Phys. J. A **34**, 405 (2007).
[37] J. Siebenson and L. Fabbietti, Phys. Rev. C **88**, 055201 (2013).
[38] K. Miyahara, T. Hyodo, and E. Oset, Phys. Rev. C **92**, 055204 (2015).
[39] T. Hyodo and D. Jido, Prog. Part. Nucl. Phys. **67**, 55 (2012).
[40] Y. Kamiya, K. Miyahara, S. Ohnishi, Y. Ikeda, T. Hyodo, E. Oset, and W. Weise, Nucl. Phys. A **954**, 41 (2016).
[41] C. Patrignani *et al.* (Particle Data Group), Chin. Phys. C **40**, 100001 (2016).
[42] L. D. Landau, Nucl. Phys. **13**, 181 (1959).
[43] S. Coleman and R. E. Norton, Nuovo Cimento **38**, 438 (1965).
[44] J. J. Wu, X. H. Liu, Q. Zhao, and B. S. Zou, Phys. Rev. Lett. **108**, 081803 (2012).

[45] F. Aceti, W. H. Liang, E. Oset, J. J. Wu, and B. S. Zou, Phys. Rev. D **86**, 114007 (2012).
[46] X. G. Wu, J. J. Wu, Q. Zhao, and B. S. Zou, Phys. Rev. D **87**, 014023 (2013).
[47] Q. Wang, C. Hanhart, and Q. Zhao, Phys. Rev. Lett. **111**, 132003 (2013).
[48] X. H. Liu and G. Li, Phys. Rev. D **88**, 014013 (2013).
[49] X. H. Liu, M. Oka, and Q. Zhao, Phys. Lett. B **753**, 297 (2016).
[50] F. K. Guo, Ulf.-G. Meißner, W. Wang, and Z. Yang, Phys. Rev. D **92**, 071502 (2015).
[51] X. H. Liu, Q. Wang, and Q. Zhao, Phys. Lett. B **757**, 231 (2016).
[52] F. K. Guo, U.-G. Meißner, J. Nieves, and Z. Yang, Eur. Phys. J. A **52**, 318 (2016).
[53] M. Bayar, F. Aceti, F. K. Guo and E. Oset, Phys. Rev. D **94**, 074039 (2016).
[54] R. Aaij *et al.* (LHCb Collaboration), Phys. Rev. Lett. **115**, 072001 (2015).
[55] X. H. Liu and U.-G. Meißner, Eur. Phys. J. C **77**, 816 (2017).
[56] S. Sakai, E. Oset, and A. Ramos, Eur. Phys. J. A **54**, 10 (2018).
[57] R. Pavao, S. Sakai, and E. Oset, Eur. Phys. J. C **77**, 599 (2017).
[58] D. Gamermann, E. Oset, D. Strottman, and M. J. Vicente Vacas, Phys. Rev. D **76**, 074016 (2007).
[59] D. Gamermann and E. Oset, Eur. Phys. J. A **33**, 119 (2007).
[60] E. Oset and A. Ramos, Eur. Phys. J. A **44**, 445 (2010).
[61] A. Ramos and E. Oset, Phys. Lett. B **727**, 287 (2013).
[62] A. Engler, H. E. Fisk, R. W. Kraemer, C. M. Meltzer, and J. B. Westgard, Phys. Rev. Lett. **15**, 224 (1965).
[63] D. W. Thomas, A. Engler, H. E. Fisk, and R. W. Kraemer, Nucl. Phys. B **56**, 15 (1973).
[64] I. Zychor *et al.*, Phys. Lett. B **660**, 167 (2008).
[65] G. Agakishiev *et al.* (HADES Collaboration), Phys. Rev. C **87**, 025201 (2013).
[66] J. Adamczewski-Musch *et al.* (HADES Collaboration), Phys. Rev. C **95**, 015207 (2017).
[67] E. J. Garzon and E. Oset, Eur. Phys. J. A **48**, 5 (2012).
[68] K. Nakamura *et al.* (Particle Data Group), J. Phys. G **37**, 075021 (2010).
[69] D. M. Manley, R. A. Arndt, Y. Goradia, and V. L. Teplitz, Phys. Rev. D **30**, 904 (1984).
[70] D. M. Manley and E. M. Saleski, Phys. Rev. D **45**, 4002 (1992).
[71] R. E. Cutkosky, C. P. Forsyth, R. E. Hendrick, and R. L. Kelly, Phys. Rev. D **20**, 2839 (1979).
[72] M. Bando, T. Kugo, and K. Yamawaki, Phys. Rep. **164**, 217 (1988).
[73] U.-G. Meissner, Phys. Rep. **161**, 213 (1988).
[74] H. Nagahiro, L. Roca, A. Hosaka, and E. Oset, Phys. Rev. D **79**, 014015 (2009).
[75] M. Bando, T. Kugo, S. Uehara, K. Yamawaki, and T. Yanagida, Phys. Rev. Lett. **54**, 1215 (1985).
[76] F. Aceti, J. M. Dias, and E. Oset, Eur. Phys. J. A **51**, 48 (2015).
[77] V. R. Debastiani, F. Aceti, W. H. Liang, and E. Oset, Phys. Rev. D **95**, 034015 (2017).
[78] F. Mandl and G. Shaw, *Quantum Field Theory* (Wiley Interscience, New York, 1984).
[79] R. P. Pavao, W. H. Liang, J. Nieves, and E. Oset, Eur. Phys. J. C **77**, 265 (2017).
[80] M. Niiyama, H. Fujimura, D. S. Ahn, J. K. Ahn, S. Ajimura, H. C. Bhang, T. H. Chang, W. C. Chang, J. Y. Chen, S. Date, S. Fukui, H. Funahashi, K. Hicks, K. Horie, T. Hotta, K. Imai, T. Ishikawa, Y. Kato, K. Kino, H. Kohri, S. Makino, T. Matsumura, T. Mibe, K. Miwa, M. Miyabe, N. Muramatsu, M. Nakamura, T. Nakano, Y. Nakatsugawa, Y. Ohashi, D. S. Oshuev, J. D. Parker, N. Saito, T. Sawada, Y. Sugaya, M. Sumihama, J. L. Tang, M. Uchida, C. W. Wang, T. Yorita, and M. Yosoi, Phys. Rev. C **78**, 035202 (2008).
[81] K. Moriya *et al.* (CLAS Collaboration), Phys. Rev. C **88**, 045201 (2013); **88**, 049902 (2013).